RESEARCH

Analysis of beat frequencies of transverse mode degeneracy in diode-pumped Nd:YVO$_4$ laser

Jing Wang[1,2] · Da Lin[1,2] · Zhanglang Lin[1] · Bingxuan Li[1] · Wenbin Liao[1] · Ge Zhang[1]

Abstract

This paper provides a detailed analysis of transverse mode degeneracy process of end-pumped Nd:YVO$_4$ laser. By observing the intersection of the beat frequency signals in the concave-plano cavity, the exact cavity length position of the transverse mode degeneracy can be clearly identified, which is also where transverse-mode locking occurs. Investigating the positions of the degeneracy of 1/3 and 2/7 reveals that transverse-mode locking occurs within the micrometer range. Our results give a simple and intuitive description of frequency degeneracy in a common solid-state laser

1 Introduction

In retrospect to the history of laser, the structured light is a significant field and it is gradually becoming mature. It is a well-known characteristic that various transverse modes could generate a structured light field through the superposition of modes in end-pumped solid-state lasers. Particularly, modulating the length of the optical resonant cavity, the transverse modes can have the same characteristic at certain specific locations [1], thereby achieving transverse mode degeneracy; the transverse mode spacing and the longitudinal mode spacing can be expressed as a ratio of two integers. This phenomenon is called frequency degeneracy. There exists a degenerate range where the gain use has high efficiency. Several reports have investigated the generation of geometric modes within a specific cavity length range in a frequency-degenerate resonant cavity. In the degenerate range resulting from cooperative frequency locking [2, 3], various patterns of transverse modes, including classical periodic orbits [4], Lissajous figures [5], 3D Lissajous parametric surfaces [6], and 3D Trochoidal parametric surfaces [7], can be observed. The precise determination of the transverse mode degeneracy range in experiments is a problem that requires meticulous control to achieve complex light field patterns.

Beat frequency signals within a laser resonator are commonly assessed using a photodiode and a radio-frequency spectrum analyzer with appropriate bandwidth experimentally. This method is used to detect the free spectral range and mode frequency difference in the resonant cavity. While established techniques involve adjusting the pump beam size or tilting the cavity mirror to modulate the output signal and assess mode-locked laser performance [8–10], we aim to investigate whether beat frequency signal changes in degenerate transverse modes remain measurable using an RF spectrum analyzer in a typical continuous-wave (CW) laser, even when the unmodulated output laser signal exhibits its random phase.

In this work, we observed the degenerate process in a concave-plano cavity without any modulation methods using a radio frequency spectrum signal analyzer. We monitored beat frequencies of various modes and analyzed their changes. We investigated the frequency difference signal tendencies near the 1/3 and 2/7-degenerate ranges. The overlap of frequency signals is a sensitive indicator of whether the resonant cavity is in the degenerate range. Additionally, we measured the degenerate range width under different pump power conditions.

Da Lin, Zhanglang Lin, Bingxuan Li, Wenbin Liao and Ge Zhang contributed equally to this work.

✉ Ge Zhang
zhg@fjirsm.ac.cn

1 Key Laboratory of Optoelectronic Materials Chemistry and Physics, Fujian Institute of Research on the Structure of Matter, Chinese Academy of Sciences, 155 Yangqiao Road West, Fuzhou 350002, Fuzhou, China

2 University of Chinese Academy of Sciences, No. 1 Yanqihu East Rd, Beijing 101408, China

2 Theory

A stable two-mirror laser resonator with the radius of curvature R_1 and R_2 of the two mirrors and the spacing L, the g parameters are expressed as $g_1 = 1 - L/R_1$, $g_2 = 1 - L/R_2$. The expression of resonant frequencies of an optical concave-plano cavity was given with the g parameters and the cavity length L [3]:

$$\Delta f_T = \frac{\Delta f_L}{\pi} cos^{-1}(g_1 g_2)^{1/2} \tag{1}$$

$$\Delta f_L = \frac{c}{2L} \tag{2}$$

$$f_{m,n,q} = q \cdot \Delta f_L + (m + n + 1) \cdot \Delta f_T \tag{3}$$

where q is the longitudinal mode index, m and n are transverse mode indexes. We obtain the longitudinal mode frequency spacing Δf_L and the transverse mode frequency spacing Δf_T. The total Gouy phase shift along the resonator could be expressed as $cos^{-1} \pm \sqrt{g_1 g_2}$. Its value must be an integer multiple of 2π after experiencing the complete round-trip paths. If r and s are integer numbers satisfy the equation $\pi^{-1} arccos(g_1 g_2)^{1/2} = r/s$, and $\Delta f_T/\Delta f_L$ equates to r/s. When the cavity satisfies the degenerate condition, some specific orders of transverse mode from each longitudinal mode exactly coincide with a discrete set of longitudinal mode frequencies of the resonator.

The mode beat frequency signals Δf_T and Δf_L can be observed [11], and the ratio of r/s can be calculated. A resonator cavity has more than one transverse mode unless using mode-selecting methods to refine the fundamental mode excited only. The beat frequencies between any two modes can be expressed as

$$\begin{aligned} f_{signal} &= f_{m_1, n_1, q_1} - f_{m_2, n_2, q_2} \\ &= [(m_1 + n_1) - (m_2 + n_2)] \cdot \Delta f_T \\ &\quad + (\Delta q_1 - \Delta q_2) \cdot \Delta f_L \\ &= (\Delta m + \Delta n) \cdot \Delta f_T + \Delta q \cdot \Delta f_L \end{aligned} \tag{4}$$

where $\Delta m + \Delta n$ is the sum of the difference between transverse-mode numbers and Δq is the difference between longitudinal-mode numbers. The f_{signal} we observed in the RF signal analyzer represents the beat frequency signal of the two modes. From this expression, we could identify the beat frequencies within the cavity. Considering the degenerate conditions of the cavity length, variations in the oscillated transverse and longitudinal modes can be inferred from changes in the RF spectrum. Our focus lies in understanding the process of transverse mode degeneracy, specifically examining the variation of the RF signal from entering the degenerate range to moving away from it.

There was a thin Nd:YVO$_4$ chip (a-cut 1.0-at.%) of which the cross-section was 5×5 mm^2 as a gain medium and it could be inserted in a concave-plano resonator (Fig. 1). The gain chip was just 0.3 mm in length. The crystal got fixed on a copper without water cooling. A collimating and focusing system comprised of two plano-convex lenses ($L_1 = 25.4$ mm, $L_2 = 75$ mm). A plano-concave lens as a pump mirror had an aperture diameter of 25.4 mm and the thickness of the lens at the center was 3 mm. The radius of curvature of the pump mirror was 50 mm. An antireflection coating at the wavelength of 808 nm is deposited on the pump mirror's two surfaces. The concave side of the pump mirror with a high reflection at the wavelength of 1064 nm. The spacing between the concave mirror and the gain medium was around 5.5 mm and the output transmission of the output mirror was 1.4% at 1064 nm. The OC had an aperture diameter of 12 mm, and the lens at the center had a thickness of 3 mm. The cavity length varied from 44 to 19 mm, with a step length of 0.01 mm. A 200 mm focal-length lens was placed 30 cm away from the output mirror. Two optical wedge prisms were used to attenuate the intensity of the beam so that we could monitor the output beam through a CCD camera (Spirincon LBA-100A), a power meter, and an RF signal analyzer (Keysight N9000A CXA). An internal preamplifier is installed on the RF. The pump beam ($M_x^2 = 26$, $M_y^2 = 18$) source was a fiber-coupled 808 nm laser diode with a core diameter of 200 μm and the numerical aperture was 0.22. After undergoing amplification via the collimation and focusing system (L_1 and L_2), the pump size incident on the gain medium measures approximately 300 μm. Our objective is to selectively excite higher-order modes, enabling subsequent observation of frequency spectrum changes using an RF analyzer. The output power was around 10 mW for the non-degenerate range and 4 mW for the degenerate range while the pump power was 2.54 W. For the pump power was 3.1 W, the output power was around 39 mW for the non-degenerate range and 36 mW for the degenerate range.
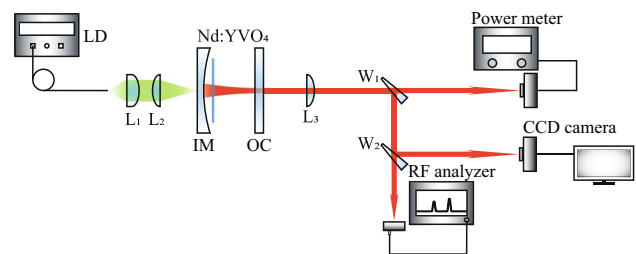

Fig. 1 Experimental setup: an Nd:YVO$_4$ crystal pumped by a 808 nm laser diode in concave-plane cavity; L_1 and L_2 are a collimating lens and a focusing lens respectively. *PM* pump mirror, *OC* output mirror, L_3 a focusing lens, W_1 and W_2 optical wedges, *CCD* charge coupled device, *RF analyzer* radio spectrum signal analyzer

3 Discussion

Noticeable signals, including beat notes generated by multi-modes, were observed in the signal analyzer. Those beat frequency signals were captured by a detector (Thorlabs Inc. DET08CL/M with a rising time of 70 ps) connected to the signal analyzer with a bandwidth of 13.5 GHz. In Fig. 2, we present the frequency signals corresponding to $\Delta f_T = 1.308$ GHz, which exhibit slightly greater strength than $\Delta f_L = 3.84$ GHz in the non-degeneracy state. The intensity beam profile corresponding to the spectrum diagram appears in the upper right corner. The pump power used in our experiment was a little above the threshold power. In general, the intensity of the beat signal of longitudinal modes is the highest peak in most spectra. Our resonant cavity contains both multiple longitudinal and multi-transverse modes, resulting in random phase relationships among the longitudinal modes without any specific frequency selection mechanism. The intensity of the beat signal serves as an indicator of the pump energy acquired by the mode. When the energy obtained by random modes within the resonant cavity decreases, the corresponding frequency difference peak also diminishes.

At a pump power of 2.54 W, we fine-tuned the cavity length to approach the 2/7 degenerate range. The theoretical optical cavity length of 30.563 mm precisely coincided with the degeneracy point of 2/7. In the frequency spectrum, we observed that as the cavity length increased, the $3\Delta f_T - \Delta f_L$ signal shifted leftward, while the $4\Delta f_T - \Delta f_L$ signal moved in the opposite direction (Fig. 3). The signal peaks of $4\Delta f_T - \Delta f_L$ and $3\Delta f_T - \Delta f_L$ overlapped. The frequency of
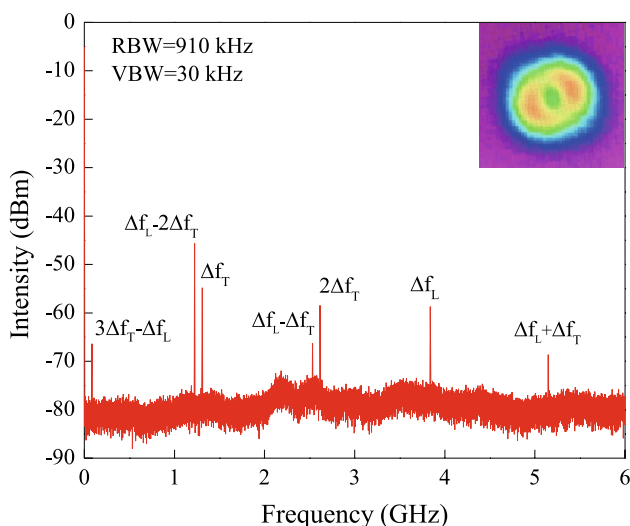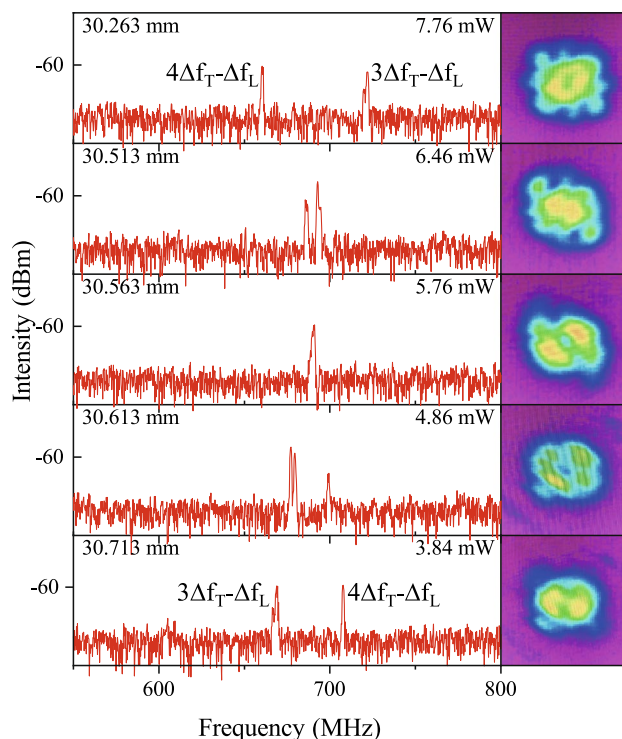

Fig. 3 The frequency spectra of $3\Delta f_T - \Delta f_L$ and $4\Delta f_T - \Delta f_L$ are plotted, corresponding to varying cavity length, output power, and beam profiles. At the degeneracy point of 2/7, the frequencies of $3\Delta f_T - \Delta f_L$ and $4\Delta f_T - \Delta f_L$ coincide

the overlapped signal was 690.4 MHz, closely matching the theoretical value of 700.64 MHz. As the cavity length increased further, the two signals diverged, and the cavity configuration moved away from the degenerate range of 2/7. Simultaneously, the signals of $6\Delta f_T - \Delta f_L$ and $\Delta f_L - \Delta f_T$ overlapped at the degeneracy point. Figure 5a illustrates the frequency variations of $\Delta f_L - 3\Delta f_T$ and $4\Delta f_T - \Delta f_L$, as well as $6\Delta f_T - \Delta f_L$ and $\Delta f_L - \Delta f_T$ with changing cavity length.

The process of transitioning into and out of the 1/3-degenerate range is also evident in the changes observed in the frequency spectrum, with a pump power of 2.54 W. Due to temperature instability during laser operation, we observe the output power drift caused by long time-constant thermal fluctuations. When the laser's output power fluctuates, the degenerate range shifts, resulting in noticeable changes in the frequency spectrum. The frequency spectra and beam profiles of 1/3-degenerate and non-degenerate states are depicted in Fig. 4. When the cavity length is outside the degenerate range, as depicted in Fig. 4a, c, the signals of $\Delta f_L - 2\Delta f_T$ and Δf_T do not overlap. Following a slight 0.59 mW increase in output power, the interval between these signals widens at a cavity length of 38.263 mm. Consequently, the degenerate point shifts from 37.513 mm (Fig. 4b) to 36.913 mm (Fig. 4d), resulting in a 0.6 mm shift. Despite this change in cavity length, the beam profile

Fig. 2 The frequency spectrum and beam profile (upper right) in the nondegenerate range of the concave-plano cavity with a 0.3 mm Nd:YVO$_4$ crystal at 2.54 W pump power

Fig. 4 The frequency spectra of $\Delta f_L - 2\Delta f_T$ and Δf_T are plotted, along with the corresponding cavity length, output power, and transverse patterns of 1/3-degenerate and non-degenerate states. **a**, **c** are the spectrum diagrams in the non-degenerate range, while **b**, **d** are the spectrum diagrams in the 1/3-degenerate range. **a**, **c** correspond to the state before the power fluctuation, whereas **b**, **d** correspond to the state after the power fluctuation. The simulation of transverse modes in the 1/3-degenerate range is given in **d**
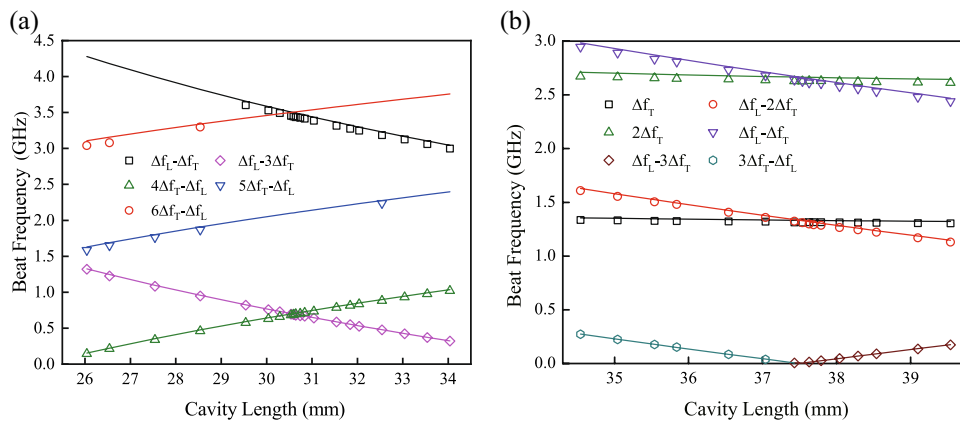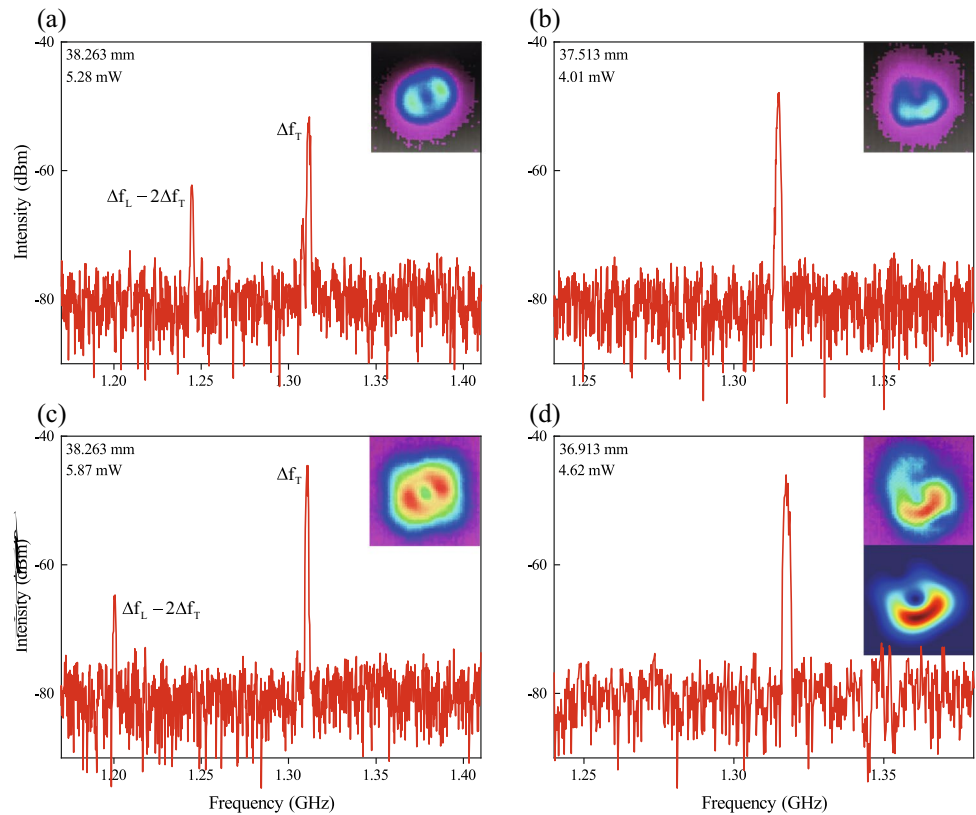
Fig. 5 **a** Beat frequency signals spanning the degenerate range of 2/7: beat frequencies of $\Delta f_L - \Delta f_T$, $\Delta f_L - 3\Delta f_T$, $4\Delta f_T - \Delta f_L$, $5\Delta f_T - \Delta f_L$, $6\Delta f_T - \Delta f_L$ with the varying cavity length. **b** Beat frequency signals spanning the degenerate range of 1/3: beat frequencies of Δf_T, $\Delta f_L - 2\Delta f_T$, $2\Delta f_T$, $\Delta f_L - \Delta f_T$, $\Delta f_L - 3\Delta f_T$, $3\Delta f_T - \Delta f_L$ with the varying cavity length. The experimental data is marked by symbols in various shapes and colors, solid lines in different colors mean numerical results of beat frequencies

at the degeneracy point remains similar. Figure 4d provides the simulation of the beam profile.

By utilizing Eq. (1) to calculate the transverse mode frequency difference as a function of cavity length, we can classify each beat note. The observed frequency variations closely matched our theoretical calculations, with only a minor discrepancy of approximately 15 MHz. The ratio r/s of frequency degeneracy corresponds to a determined

cavity length in our cavity. In Fig. 5, the frequency degeneracy point is visually represented as the intersection of frequency signal curves. All signals observed in RF can be correlated to theoretical curves. The variation of beat frequency signals with cavity length across the degenerate range of 2/7 is illustrated in Fig. 5a, and the beat frequencies spanning the degenerate range of 1/3 are shown in Fig. 5b.

Theoretically, the $3\Delta f_T - \Delta f_L$ beat frequency reaches zero at the 1/3-degeneracy point (Fig. 5b). However, in practical measurements, the $3\Delta f_T - \Delta f_L$ signal typically disappears as the cavity length approaches the degenerate range. This phenomenon can be attributed to the effect of spatial hole burning within the population inversion distribution [12]. To determine the degenerate region we observed other stable signals near the 1/3-degenerate range (such as $\Delta f_L - 2\Delta f_T$ and Δf_T, $\Delta f_L - \Delta f_T$ and $2\Delta f_T$). Figure 6 illustrates the variation in spacing between the $\Delta f_L - 2\Delta f_T$ and Δf_T signal peaks near the 1/3-degenerate range (both experimentally and theoretically), along with the corresponding power curve at the pump power of 3.1 W. When the cavity length falls within the range of 37.463 to 37.556 mm, the two signal peaks overlap, yielding a synthesized signal peak width between 3.4 and 4.5 MHz. At a pump power of 3.1 W, the cavity length corresponding to the signal intersection point defines the width of the 1/3 degenerate range, which measures 55 μm. Table 1 presents the measured degenerate range widths across various pump powers, ranging from 15 to 100 μm. It should be noted that the width of the degenerate range was not associated with pump energy.

4 Conclusion

Our research details the process of beat frequency signals for 1/3 and 2/7-degenerate ranges. Beat frequency signals change within and out of the degenerate range, which can be monitored using an RF signal analyzer. Monitoring the beat frequency signals allows precise measurement of the cavity
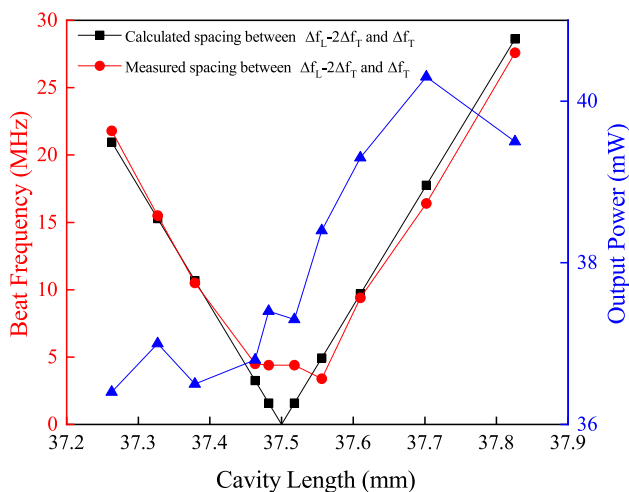
Table 1 Width of the 1/3-degenerate range measured at various pump powers

Pump power (W)	Degenerate range width (μm)
0.98	37
1.25	33
1.51	31
1.78	49
2.05	80
2.58	26
3.1	55
3.64	18

length movement at the degeneracy point due to the output power fluctuations. The transverse mode patterns closely correspond to the frequency spectra within the degenerate and non-degenerate ranges. Using the RF signal analyzer, we can determine the position of the degenerate range and interval width. The degenerate range width ranges from approximately 15–100 μm and shows no correlation with pump energy.

Declarations

Fig. 6 The variation in spacing between the frequency signals $\Delta f_L - 2\Delta f_T$ and Δf_T at the 1/3-degeneracy was illustrated in theoretical and experimental results. Transverse mode degeneracy is observed when this spacing approaches zero. The output power varied with cavity length near the degenerate range

References

1. T. Klaassen, J. Jong, M. Exter, J. Woerdman, Transverse mode coupling in an optical resonator. Opt. Lett. **30**(15), 1959–1961 (2005)

2. L. Lugiato, C. Oldano, L. Narducci, Cooperative frequency locking and stationary spatial structures in lasers. JOSA B **5**(5), 879–888 (1988)

3. Y.-F. Chen, K.-F. Huang, Y.-P. Lan, Spontaneous transverse patterns in a microchip laser with a frequency-degenerate resonator. Opt. Lett. **28**(19), 1811–1813 (2003)

4. Y.-F. Chen, K.-F. Huang, Y.-P. Lan, Localization of wave patterns on classical periodic orbits in a square billiard. Phys. Rev. E **66**(4), 046215 (2002)

5. Y.-F. Chen, Y.-P. Lan, K.-F. Huang, Observation of quantum-classical correspondence from high-order transverse patterns. Phys. Rev. A **68**(4), 043803 (2003)

6. Y.-F. Chen, T.-H. Lu, K.-W. Su, K.-F. Huang, Devil's staircase in three-dimensional coherent waves localized on Lissajous parametric surfaces. Phys. Rev. Lett. **96**(21), 213902 (2006)

7. T.-H. Lu, Y. Lin, Y.-F. Chen, K.-F. Huang, Three-dimensional coherent optical waves localized on trochoidal parametric surfaces. Phys. Rev. Lett. **101**(23), 233901 (2008)

8. C.-C. Hsu, J.-H. Lin, W.-F. Hsieh, Pulse-train modulation in a picosecond self-mode-locked laser. J. Phys. B Atom. Mol. Opt. Phys. **42**(14), 145402 (2009)

9. Y. Kohanzadeh, D. Auston, Measurement of low-absorption coefficients using the beat frequency shift between transverse modes of a laser. IEEE J. Quantum Electron. **6**(7), 475–477 (1970)

10. C.-W. Chen, Y.-H. Fang, C.-Y. Cho, H.-C. Liang, Investigation of anisotropic thermal lens effect in a dual-polarized Nd:Ylf laser. Opt. Lett. **46**(1), 94–97 (2021)

11. C. Tsou, H. Liang, K.-F. Huang, Y.-F. Chen, Various phenomena of self-mode-locked operation in optically pumped semiconductor lasers. In: Vertical External Cavity Surface Emitting Lasers (VECSELs) VII, vol. 10087 (International Society for Optics and Photonics, 2017), p. 100870

12. T. Kimura, K. Otsuka, M. Saruwatari, Spatial hole-burning effects in a Nd^{3+}:Yag laser. IEEE J. Quantum Electron. **7**(6), 225–230 (1971)